RSC Advances

This is an *Accepted Manuscript*, which has been through the Royal Society of Chemistry peer review process and has been accepted for publication.

Accepted Manuscripts are published online shortly after acceptance, before technical editing, formatting and proof reading. Using this free service, authors can make their results available to the community, in citable form, before we publish the edited article. This *Accepted Manuscript* will be replaced by the edited, formatted and paginated article as soon as this is available.

You can find more information about *Accepted Manuscripts* in the Information for Authors.

Please note that technical editing may introduce minor changes to the text and/or graphics, which may alter content. The journal's standard Terms & Conditions and the Ethical guidelines still apply. In no event shall the Royal Society of Chemistry be held responsible for any errors or omissions in this *Accepted Manuscript* or any consequences arising from the use of any information it contains.

ROYAL SOCIETY OF CHEMISTRY

www.rsc.org/advances

RSC Advances RSCPublishing

ARTICLE

Cite this: DOI: 10.1039/x0xx00000x

Received 13th June 2014,
Accepted 13th August 2014

DOI: 10.1039/x0xx00000x

www.rsc.org/

Interfacial mechanical testing of atomic layer deposited TiO_2 and Al_2O_3 on silicon substrate by the use of embedded SiO_2 microspheres

*J. Lyytinen [a], M. Berdova [a,b], P. Hirvonen [a], X.W. Liu [a], S. Franssila [a,b], Q. Zhou [c] and J. Koskinen [a] ,

In this paper the authors present a next generation measurement system for interfacial mechanical testing of especially atomic layer deposited (ALD) thin films. SiO_2 microspheres were embedded in 100 and 300 nm thick ALD TiO_2 and Al_2O_3, deposited at 110°C, 200°C and 300°C on a silicon substrate. The embedded microspheres were detached using a fully programmable semi-automatic microrobotic assembly station employed to carry out the lateral pushing and detaching force ***F* (µN)** measurement. The area of interfacial fracture ***A* (µm²)** was measured using scanning electron microscopy and digital image analysis to calculate critical stress of interfacial fracture ***σ* (MPa)**. Work ***W* (J)** and energy release rate ***G* (J/m²)** of interfacial fracture were also calculated from the measurement results. Interfacial fracture from the film-substrate interface occurred only for TiO_2 deposited at 200°C which had crystalline structure with the biggest grain size, signifying that for all of the other samples, film adhesion was excellent, and significantly better than film cohesion. Quantitatively this means that thin film interfacial adhesion to the substrate was also higher than the values of the critical stresses and the measured energy release rates. Interfacial toughness seems to be related to film thickness and crystallinity in the case of TiO_2, but with Al_2O_3 the interfacial toughness seems to increase with the deposition temperature. The method presented in this paper is generic, and can be applied for the evaluation of interfacial mechanical properties, such as adhesion, between any various film-substrate-sphere system of choice.

Introduction

Atomic layer deposition (ALD) can produce highly conformal and defect free coatings that are typically used in semiconductor devices, micro-/nanoelectromechanical systems (MEMS/NEMS) and energy applications.[1-3] Thin film functional characteristics, performance and practical usability are highly dependent on sufficient interfacial mechanical properties such as the adhesion between the film and the substrate as well as the cohesion of the film.[4] Conventional interfacial mechanical testing methods for thin films include scratch-testing, pull-off-testing, peel-testing and bend-testing to name a few.[4-6] However, there is no universal technique for determining interfacial toughness as test-specific factors and residual stress affect the measured adhesion and interfacial properties.[4] The results of different testing methods for interfacial properties are not easily comparable and can often give only qualitative or comparative results.[7] Especially in the case of strongly adhering thin films with good interfacial mechanical properties there can be problems when using conventional methods. For example in scratch testing the substrate can break before the film is delaminated[8] and quantitative analysis of adhesion, which is required to build reliable devices, is problematic for many tests. Overall, the characterization of interfacial mechanical properties of increasingly thinner films is challenging with many practical shortcomings and thus method development is needed to be able to characterize and produce thin films with improved interfacial mechanical properties.

New approaches to study interfacial mechanical properties of ALD thin films include shaft-loading blister testing[9] and scanning nanowear[8]. Matoy *et al.* studied interface fracture properties of silicon oxide and metallic thin films by deflecting microcantilevers fabricated by focused ion beam machining[10] that has similar test geometry as in our embedded microsphere test structure. Latella *et al.* studied cracking and interfacial

RSC Advances Accepted Manuscript

This journal is © The Royal Society of Chemistry 2014

adhesion characteristics of 140 nm ALD Al_2O_3 deposited in 100°C on a polycarbonate (PC) substrate using bend testing and measured critical stress for cracking of the alumina films of $\sigma_c = 140 \pm 3$ MPa and fracture energies of 11-34 J/m^2.[11]
A new adhesion test method to study the interfacial mechanical properties of ALD thin films by the use of embedded microspheres was reported earlier.[12] In this paper the authors present a next generation measurement system for interfacial mechanical testing of especially ALD thin films by the use of embedded SiO_2 microspheres developed further from the previous system. The method is generic, and can be applied for the evaluation of interfacial mechanical properties, such as adhesion, between any various film-substrate-sphere system of choice.

Experimental

Sample fabrication

SiO_2 microspheres with the vendor specified average diameter of 8 µm (with a coefficient of variation <10%) purchased from Cospheric LLC were dry-deposited in a clean room environment on RCA cleaned (100)-silicon by aerosol deposition. The microspheres were then embedded in twelve different types of ALD layers. Five microspheres were measured per sample type resulting in a total number of 60 samples.

The (100) single-side polished (SSP) silicon substrate (150 mm wafers) were wet cleaned before the film growth using RCA - cleaning sequence (SC-1, HF-dip and SC-2). SC-1 is a mixture of deionized water, ammonia and hydrogen peroxide (H_2O:NH_3:H_2O_2 5:1:1) and wafers were kept there for 10 minutes at 65°C with megasonic on, wafers were dipped in HF (H_2O:HF(50%) 50:1) for 30 seconds (at room temperature) and finally in SC-2,which is an mixture of deionized water, ammonium hydroxide and hydrogen peroxide (H_2O:NH_4OH:H_2O_2 5:1:1) for 10 minutes at 65°C. After cleaning, the wafers were covered with a thin, about 1 - 2 nm thick chemical oxide (SiO_x).

Experimental matrix (Table 1) consists of two different materials: Al_2O_3 (sample code A) and TiO_2 (sample code T), three different deposition temperatures: 110±5°C (sample code L/low), 200±5°C (sample code M/medium) and 300±5°C (sample code H/high) and two different film thicknesses: 100 nm (sample code 100) and 300 nm (sample code 300) resulting in 12 different sample types. (For example the sample code TM300 would mean 300 nm TiO_2 deposited at 200°C).

Table 1. Experimental matrix of different sample types

Sample code	Material	Deposition temperature (°C)	Target thickness (nm)
TL100	TiO2	110	100
TM100	TiO2	200	100
TH100	TiO2	300	100
AL100	Al2O3	110	100
AM100	Al2O3	200	100
AH100	Al2O3	300	100
TL300	TiO2	110	300
TM300	TiO2	200	300
TH300	TiO2	300	300
AL300	Al2O3	110	300
AM300	Al2O3	200	300
AH300	Al2O3	300	300

TiO_2 was deposited from $TiCl_4$ and deionized water (H_2O) precursors with the following pulsing sequence: 0.2 s water pulse – 0.3 s $TiCl_4$ pulse – 0.5 s N_2 purge – 1.5 s waiting time. Al_2O_3 was deposited from trimethylaluminum (TMA) and H_2O precursors with the following pulsing sequence: 0.25 s TMA pulse - 0.75 s N_2 purge - 0.2 s H_2O pulse - 0.75 s N_2 purge. All of the depositions were done using Beneq-TFS500 reactor at Micronova Nanofabrication Center of Aalto University.

Sample properties

Typical values for hardness, Young's modulus, Poisson's ratio, crystallinity and chemical composition have been measured before for similar films and they are listed here for comparison. The experimental procedures are explained in prior publications.[8, 13, 14] The grain size has been measured for the films deposited in this paper using SEM and imageJ digital image analysis software.

Hardness, Young's Modulus, Poisson's Ratio and Residual Stress

Typical values for hardness, Young's modulus, Poisson's ratio and residual stress for similar thin films can be found in Table 2 for comparison.

RSC Advances Accepted Manuscript

This journal is © The Royal Society of Chemistry 2014

Table 2. Typical values for hardness, Young's modulus, Poisson's ratio and residual stress of similar TiO_2 and Al_2O_3 thin films.[8, 13,14]

Sample	Hardness (GPa)	Young's modulus (MPa)	Poisson's ratio	Residual stress (MPa)
TL100	6.9 ± 0.1	152.2	0.28	415±35
TM100	8.5 ± 1.0	154.4	0.28	625±225
TH100	9.7 ± 1.0	155.0	0.28	455±55
AL100	7.9 ± 0.2	138.5	0.24	555±25
AM100	9.8 ± 0.3	166.6	0.24	450±20
AH100	10.5 ± 0.5	169.8	0.24	180±60
TL300	6.9 ± 0.1	152.2	0.28	415±35
TM300	8.5 ± 1.0	154.4	0.28	625±225
TH300	9.7 ± 1.0	155.0	0.28	455±55
AL300	7.9 ± 0.2	138.5	0.24	555±25
AM300	9.8 ± 0.3	166.6	0.24	450±20
AH300	10.5 ± 0.5	169.8	0.24	180±60

Crystallinity, grain size and chemical composition

Typical values of thin film crystallinity measured by grazing incidence X-ray diffraction (GIXRD) and chemical composition measured by time-of-flight elastic-recoil detection analysis (TOF-ERDA) can be found in Table 3.

Table 3. Typical values for thin film crystallinity and chemical composition measured by TOF-ERDA. *=Crystalline/Phase. †TM300 has a dual scale grain size with main crystalline size of 0,90±0.25 µm and a secondary crystalline size of 0.23±0.06 µm.[8, 13, 14]

Sample	Crystallinity	Grain size (µm)	Stoichiometry	H%
TL100	Amorphous	-	Ti:O 1:2	3,7 ± 0.05
TM100	*/Anatase	0.25±0.05	Ti:O 1:2	3,85 ± 0.05
TH100	*/Anatase	0.10±0.02	Ti:O 1:2	3,85 ± 0.05
AL100	Amorphous	-	Al:O 1:1.15	11.3 ± 1.1
AM100	Amorphous	-	Al:O 1:1.15	2.5 ± 0.3
AH100	Amorphous	-	Al:O 1:1.15	1.0 ± 0.1
TL300	Amorphous	-	Ti:O 1:2	3,7 ± 0.05
TM300	*/Anatase	†0.90±0.25 / 0.23±0.06	Ti:O 1:2	3,85 ± 0.05
TH300	*/Anatase	0.11±0.06	Ti:O 1:2	3,85 ± 0.05
AL300	Amorphous	-	Al:O 1:1.15	11.3 ± 1.1
AM300	Amorphous	-	Al:O 1:1.15	2.5 ± 0.3
AH300	Amorphous	-	Al:O 1:1.15	1.0 ± 0.1

Measurement system

The microrobotic assembly station employed to carry out the lateral pushing and detaching force measurement consisted of the following components: top and side view microscopes (allowing the measurement of opaque substrates such as silicon) for sample positioning and video recording of the measurements, X/Y/Rotational stage for sample movement (Physik Instrumente, M-404.8PD, M-122.2DD, M-116.DG, respectively), commercial microforce sensing probes for detaching force measurement (FemtoTools, FT-S1000 and FT-S10000) that were attached to a vertical positioning stage (Physik Instrumente, M-122.2DD) via an adapter piece that also allowed angle adjustment. The sensor was mounted at an angle of 12° resulting in a force coefficient of cos 12° = 0.98.

The FT-S1000 sensor (±1000 µN force range, 0.05 µN resolution) was used to measure 100 nm thick samples and the FT-S10000 sensor (±10000 µN force range, 0.5 µN resolution) was used to measure 300 nm thick samples. A sampling rate of 1 kHz in the measurements enabled the acquisition of the fast dynamics of the microsphere detachment allowing the analysis of work and energy release rate of interfacial fracture. The sensor tip height was adjusted manually. The tip was lowered as close to the surface as possible while trying to avoid contact. The stage was driven at a constant speed of 10 µm/s against the force sensor during the measurements. The measurement were done semi-automatically with a fully programmable measurement script that controlled the stages as well as the force acquisition. The automated measurement program increases the repeatability and reliability of the test method.

Characterization with AFM, SEM and digital image analysis

AFM

PSIA XE-100 Advanced Scanning Probe Microscope was used for atomic force microscopy (AFM) in tapping mode with suitable scanning areas related to the specific areas of interfacial fracture to confirm film-substrate delamination and to study the topographical features of especially unclear fractured surfaces and interfaces after the detaching force measurements.

SEM

The samples were imaged with TESCAN MIRA3 FEG-SEM before and after the lateral force measurement. Microspheres were identified and their coordinates were recorded to find each individual microsphere before and after the measurement.

Digital Image Analysis

The area of interfacial fracture was masked with Adobe Photoshop and the area was measured with ImageJ digital image analysis software.[15]

Modeling

The embedded microsphere structure was further examined using Finite Element Analysis (FEA) to model the multiaxial stress state and stress distribution.

This inspection was carried out with commercial FEA software COMSOL Multiphysics (v. 4.3b). The computation was performed on Aalto University Ubuntu shell servers for light computing; both equipped with 16 CPU cores and 256 GB RAM. A non-transient, static analysis was chosen that allowed for geometrical nonlinearity. The used material model was linear elastic and discretization of solved displacement field was specified as quadratic. The modeled and meshed geometry is demonstrated in Figure 1. Due to the obvious geometrical symmetry present in the experiments, it was possible to halve the model and hence also the computational effort. For the silica sphere, a radius of 4 µm was used, and modeled thin film thicknesses were 100 and 300 nm.

RSC Advances Accepted Manuscript

Multiple-shaped mesh elements, e.g. tetrahedral, prismatic and hexahedral, were exploited in order to achieve suitable meshing. By a suitable mesh we mean one with sufficient resolution in regions of interest but still having enough sparsity in non-critical regions, to yield a computationally reasonable cost-efficiency. A further target for the mesh was to be geometrically well-defined, thus resulting in robustness of both mesh generation and convergence of solution procedure; despite alteration of design parameters and loading, respectively. Comparison with solutions given by a denser mesh resulted in good agreement of relevant stress data, which was taken as confirmation of adequate mesh quality.[16]

Material properties in the model were assumed homogeneous, and their variation abrupt over material interfaces. The experimentally measured values were utilized in the simulation and thin film mechanical properties are given, along with loading parameters, in Table 4. Elastic moduli of 150 and 70 GPa were assigned to silicon substrate and silica sphere, respectively, whereas a Poisson's ratio of 0.17 was set for both. The effect of silicon substrate anisotropicity was investigated by repeatedly evaluating a simulation case with varying orientation of anisotropicity. As the difference in relevant stress data between different orientation cases was negligible, all materials were modeled as isotropic.

A symmetry boundary condition was applied to the whole cross-section of the halved geometry. The bottom of the substrate as well as the cylindrical walls of the substrate and the thin film were set fixed. Due to its relatively minor effect on computational cost, the included portion of substrate was modeled exaggeratedly large. Also, after Saint-Venant's principle and our interest focusing on the neck region, the loading was applied as a normal point force at 12° inclination. An exception was made for the highest-loaded case (TL300) where a distributed load had to be used to find a solution. The forces applied in the simulations equal the experimentally determined average detaching forces for investigation of critical stress fields. Fixed boundary condition and the point loading are also given in Figure 1.

Table 4. Loading and material parameters utilized in the simulations, namely load magnitude, and elastic moduli and Poisson's ratios for the thin films. Elastic moduli of silicon and silica were 150 and 70 GPa, respectively. Poisson's ratio for both was 0.17.

Modeling case	load (μN)	E_film (GPa)	vfilm (1)
TL100	196.5	152.2	0.28
TM100	182.2	154.4	0.28
TH100	171.4	155.0	0.28
AL100	138.0	138.5	0.24
AM100	170.7	166.6	0.24
AH100	125.7	169.8	0.24
TL300	1219.5	152.2	0.28
TM300	864.9	154.4	0.28
TH300	811.6	155.0	0.28
AL300	595.3	138.5	0.24
AM300	708.9	166.6	0.24
AH300	764.2	169.8	0.24

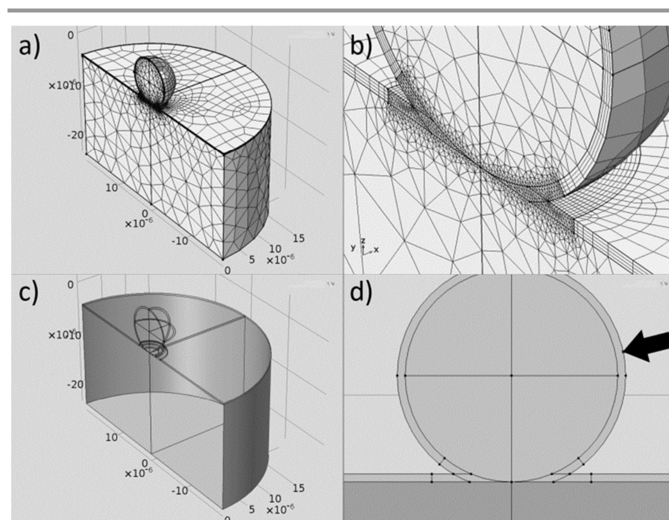

Figure 1. Finite element model of the embedded microsphere system. a), b) Geometry with 300 nm thin film thickness fully meshed displaying multiple-shaped mesh elements. The mesh proved cost-effective and robust in practice. c) Fixed boundaries and d) application point of point force highlighted with an arrow.

Analysis of interfacial mechanical properties

DETACHING FORCE, F

The detaching force, F (μN), was measured as the difference between the average zero-load voltage and the measured voltage (ΔV) when detaching the sphere (as shown in Figure 2). Conversion to μN was done by multiplying the ΔV with the sensor calibration coefficient or gain of the sensor (μN/V). The measured forces were in the range of 150 – 1600 μN.

RSC Advances Accepted Manuscript

 This journal is © The Royal Society of Chemistry 2014

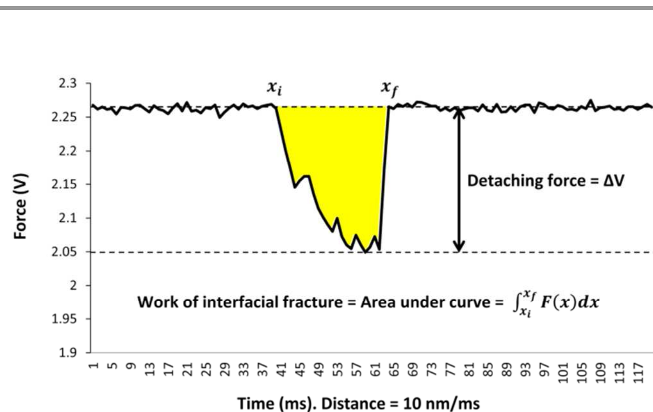

Figure 2 (color online). Example of detaching force measurement. Detaching force is calculated as ΔV from the average zero-load voltage and the measured voltage. Conversion to μN is done by using the sensor calibration coefficient or gain of the sensor (μN/V). The Work of interfacial fracture or the detaching energy was calculated as the area under the curve F(x) from the measurement results.

Area of Interfacial Fracture, A

The area of interfacial fracture, A (μm^2), was measured from the SEM images. First, area masking was done using Adobe Photoshop, and then the area was measured using ImageJ digital image analysis software. The measured areas of interfacial fracture were in the range of 3 – 22 μm^2.

Critical Stress of Interfacial Fracture, σ

The critical stress of interfacial fracture σ (MPa) was calculated as $F/$A (the detaching force F divided by the area of interfacial fracture A). The measured critical stresses were in the range of 25 – 70 MPa.

Work of Interfacial Fracture, W

The work of interfacial fracture, W (pJ), or the detaching energy was calculated from the force measurement graph when detaching the spheres. The average zero-load voltage was set as the origin of the x axis, and the measured voltage was set as the function F(x). The work of interfacial fracture was then integrated as the area between the function F(x) curve and the x axis, between the limits x_i (starting point of interfacial fracture) and x_f (ending point of interfacial fracture) as shown in Figure 2). The measured works of interfacial fracture were in the range of 4 – 177 pJ.

Energy Release Rate of Interfacial Fracture, G

The energy release rate of interfacial fracture, G (J/m^2) was calculated as W/A (the work of interfacial fracture W divided by the area of interfacial fracture A). The measured energy release rates of fracture were in the range of 1.3 – 8.6 J/m^2.

Results and discussion

AFM analysis

AFM results explained irregularities in SEM images and showed hole topography. AFM measurement confirmed that the sample TM300 was the only film with interfacial fracture from the film-substrate interface as is shown in Figure 3. signifying lower interfacial film-substrate adhesion compared to all of the other samples.

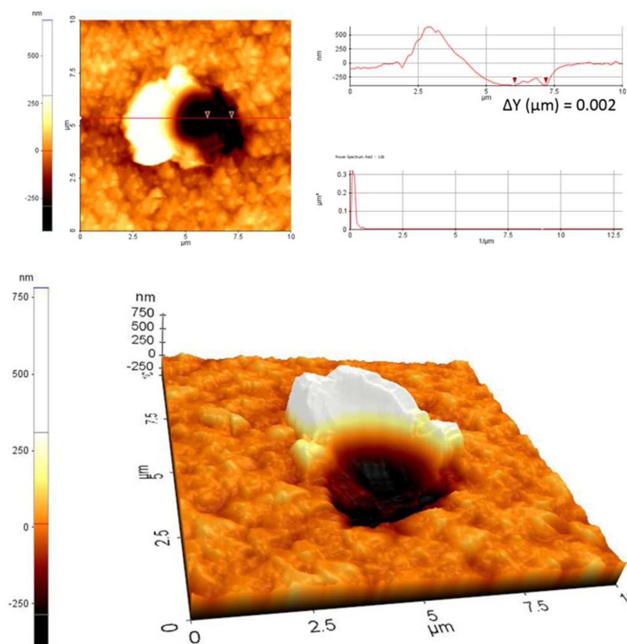

Figure 3 (color online). AFM measurement confirmed that the sample TM300 was the only film with interfacial fracture from the film-substrate interface signifying lower interfacial adhesion compared to all of the other samples. The y-axis difference marked with the arrows between the location of the sphere bottom and the delaminated film was 2 nm.

SEM characterization for area calculation and digital image analysis

Typical SEM-images of interfacial fracture from different 100 nm thick samples can be seen in Figure 4.

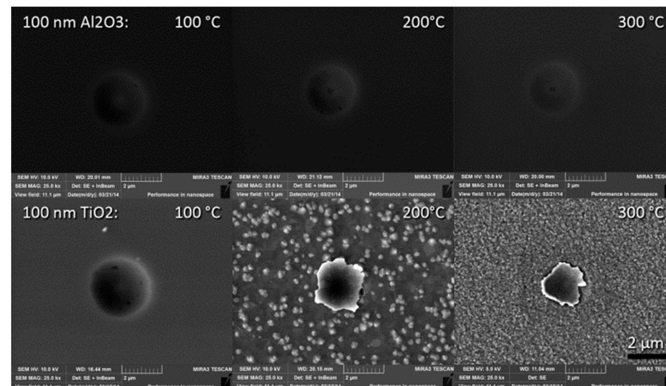

Figure 4. SEM images of 100 nm thick samples after testing.

Typical SEM-images of interfacial fracture from different 300 nm thick samples can be seen in Figure 5.

RSC Advances Accepted Manuscript

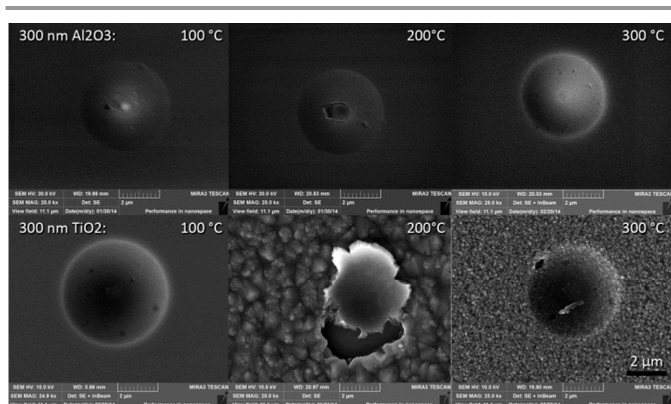

Figure 5. SEM images of 300 nm thick samples after testing.

Modeling

Figure 6 depicts the von Mises stress in the test structure coded TH300. Besides the point of load application, largest stress concentrations occur in the neck region shown especially in Figure 6 b) and c), which we are more interested in. The stress maximum is located near the symmetry plane and, depending on modeling case, either on negative y-axis side (tension in z-direction) or positive y-axis side (compression in z-direction). A further clarification is given in Figure 6 d) that reveals two-dimensional stress distribution along both substrate-thin film and sphere-thin film interfaces. The maximum is located very near the symmetry plane and is roughly equal on negative y-axis side (tension in z-direction) and positive y-axis side (compression in z-direction). These maximum values shoot off to gigapascals because of linear continuum elasticity predicting stress behavior $\sigma \propto r^{-1/2}$ in vicinity of a crack tip. Thus, we set the maximum of stress scale to a more modest 500 MPa, which better demonstrates distribution of stress.

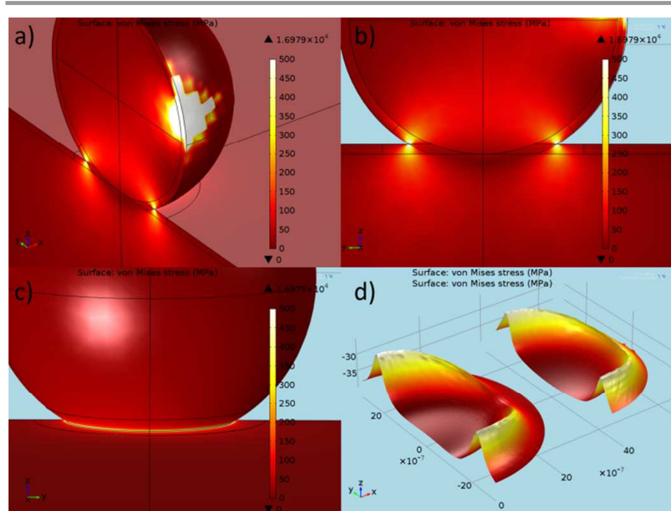

Figure 6 (color online). Loading induced stress in TH300 case represented by von Mises stress. a) Overview of the microsphere stress distribution, b) a close-up of cross-section at neck region, c) stress concentration at the neck edge from the opposite side and d) 2D stress distributions along substrate-thin film (bottom-left) and sphere-thin film (top-right) interfaces where z-coordinates have been replaced with von Mises stress values (arbitrary units).

Stress tensor component data was extracted in the symmetry plane, along the film-substrate and the film-sphere interfaces — not at the neck edge tips to circumvent the stress singularities. Data extraction paths are highlighted (in blue online) in Figure 7 a) and b). Furthermore, these interfaces are of most interest for the present study. Corresponding data is plotted in Figure 7 c) and d), respectively. Stress components negligible in magnitude have been omitted.

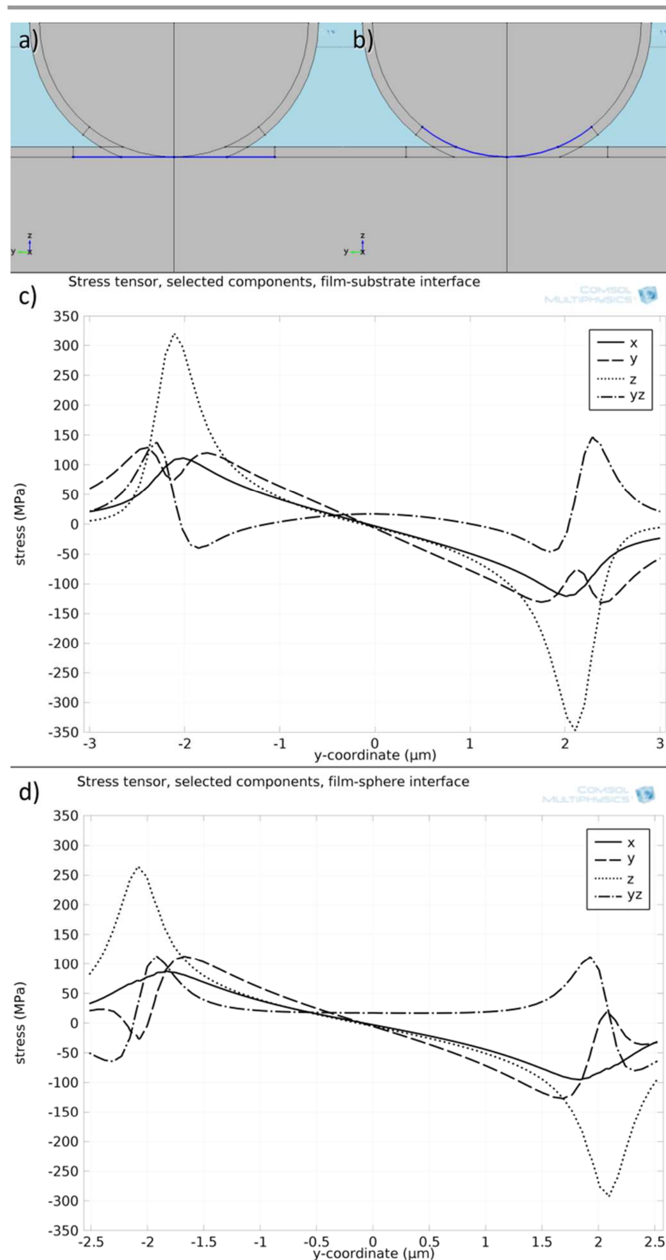

Figure 7 (color online). a) film-substrate interface, b) film-sphere interface, c) multiaxial stresses of film-substrate interface and d) multiaxial stresses of film-sphere interface.

Depending on stress tensor component, the curves are rather symmetrical or antisymmetrical. Stresses rise up to several megapascals with stress tensor z-component being the largest in magnitude. The shear component yz may also be significant for

RSC Advances Accepted Manuscript

This journal is © The Royal Society of Chemistry 2014

fracture. Interestingly, it appears that there is some difference in magnitude of the stress components between the interfaces, and this is in favor of the film-substrate interface. While the exact shape and height of formed stress curves varied, the observations made above apply to all simulation results obtained.

Interfacial mechanical analysis

The elastic modulus and hardness of the silica microspheres is in the region of 68.9 ± 9.6 GPa and 2.8 ± 0.4 GPa respectively. The microspheres are durable and stiff. At no point did the microspheres break.[17]

Detaching force

The detaching force results can be found in Figure 8.

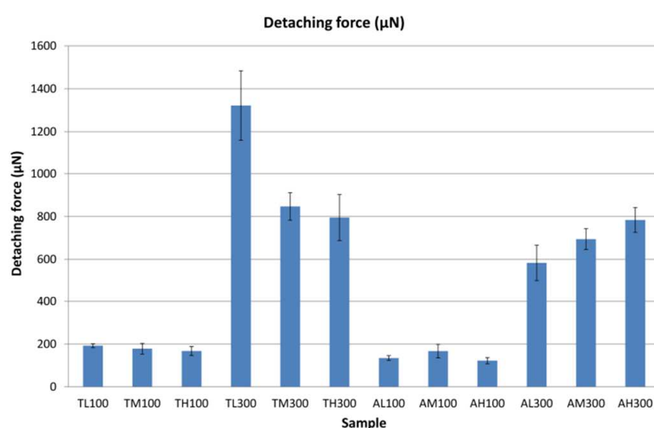

Figure 8 (color online). Detaching force results

For all of the samples film thickness increased the detaching force significantly due to film cohesion. The sample TL300 had significantly highest detaching force value probably due to the fact that the it was amorphous compared to the crystalline samples TM300 and TH300. With alumina the detaching force increased in a linear-like fashion probably due to increased thin film hardness increasing the mechanical durability of interfacial fracture.

Area of Interfacial Fracture

The areas of interfacial fracture can be found in Figure 9.

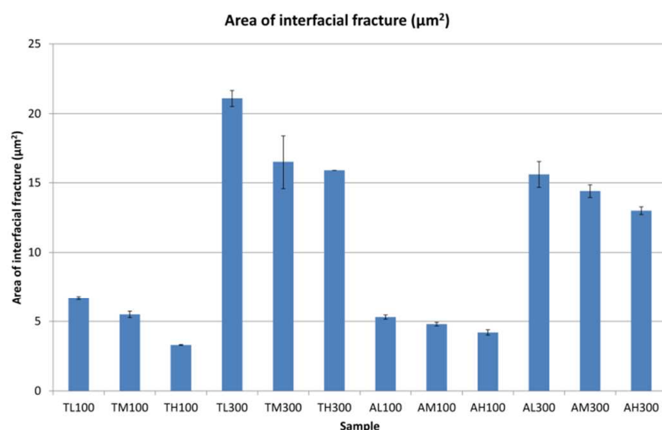

Figure 9 (color online). Area of interfacial fracture (μm^2)

The deposition temperature seemed to have an adverse effect on the area of interfacial fracture: the higher the deposition temperature, the lower the area of interfacial fracture. This might be due to increased hardness that causes higher mechanical resistance to fracture.

Critical Stress of Interfacial Fracture

The results of the critical stress of the interfacial fracture calculation can be found in Figure 10.

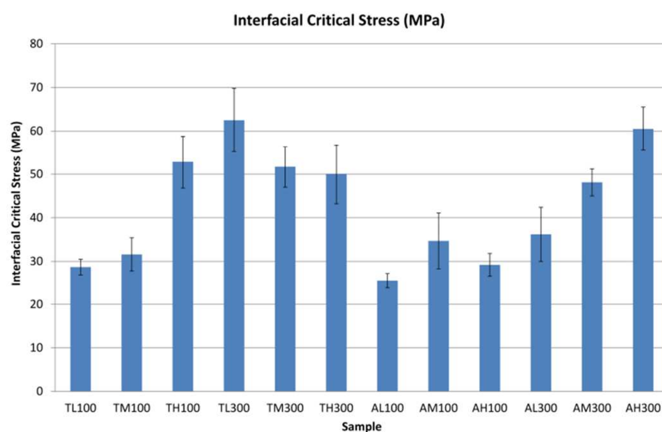

Figure 10 (color online). Critical Stress of Interfacial Fracture (MPa).

Interfacial fracture occurred from the film-sphere interface or as cohesive failure from all of the other samples besides TM300. This signifies that the film-substrate adhesion is higher than film cohesion in all of the cases but 300 nm TiO_2 grown at 200°C, which is the only sample that showed classic delamination or interfacial fracture from the film-substrate interface. Crystallinity and grain size play a big role in the interfacial durability, the sample TM300 was crystalline and had the biggest grain size as seen in Figure 5. The interfacial fracture from the film-substrate interface was brittle-type fracture, where the large crystal size caused less mechanical resistance to fracture compared to samples with smaller crystal size or samples which were amorphous. Of the TiO_2 samples

RSC Advances Accepted Manuscript

TL300 (110°C, 300 nm) had the highest mechanical durability. This is most probably due to the fact that the sample is amorphous. However TH100 had the highest mechanical durability with 100 nm thick TiO_2 samples. TiO_2 deposited at 300°C had highest hardness, and a small crystal size of 0.1±0.02 µm (nearing amorphous structure) as seen in Figure 4. This signifies that crystallinity and film thickness have an effect on interfacial durability.

Puurunen *et al.* studied the adhesion of TiO_2 to SiO_2, but they used significantly thinner films of about 10 nm and annealing up to 1100°C resulting in non-continous Ti-containing layers as well as a different measurement method. The resulting TiO_2-SiO_2 adhesion measured with pull test was 23 MPa, which is lower than our results. For plasma-activated samples annealed at 200°C the resulting pull strength was in the range of 8 MPa, but again the film thickness was only a fraction of the film thicknesses in this paper.[18] Also, our results include the effect of film cohesion, so the critical stress value of pure adhesion is even lower than the measured values.

With Al_2O_3 the sample AH300 had the highest interfacial critical stress value. With 300 nm samples the interfacial mechanical durability increases in a linear-like fashion with the deposition temperature. With 100 nm samples all of the results are within error limits, although the 200°C sample has the highest average value (but also the largest standard deviation) of all of the 100 nm samples. With alumina, all of the samples are amorphous, and the main factor related to mechanical durability seems to be film hardness combined with lower residual stress as listed in Table 2.

Work of Interfacial Fracture

The results of the calculation for work of interfacial fracture can be found in Figure 11.

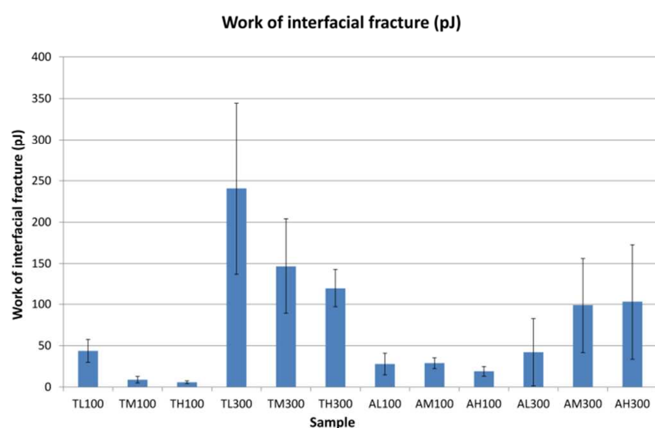

Figure 11 (color online). Work of interfacial fracture.

Sample TL300 had clearly the highest value for the work of interfacial fracture, although the standard deviation was also the highest. With TiO_2, film thickness increased the work of interfacial fracture due to film cohesion, as there is more material to be fractured which consumes more energy. The work of interfacial fracture had a decreasing trend with increasing the deposition temperature probably due to film crystallinity. With Al_2O_3, film thickness increased the work of interfacial failure due to film cohesion. However, there was no significant effect with deposition temperature as all of the results were within standard deviation of each other.

Energy Release Rate of Interfacial Fracture

The results of the calculation of energy release rate of fracture can be found in Figure 12.

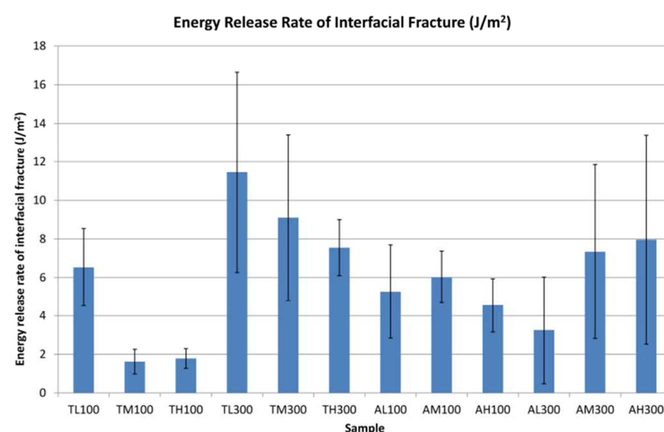

Figure 12 (color online). Energy release rate of interfacial fracture (J/m^2).

The sample TL300 had the highest energy release rate of interfacial fracture and the value decreased with increasing the deposition temperature probably due to film crystallinity, although with higher temperatures the standard deviation was lower signifying a more homogenous film. With alumina all of the samples are amorphous and the difference was not so clear. The trend of energy release rate with increasing the deposition temperature was nearly linear, however the AM300 and AH300 had slightly higher average values.

Summary of Results

A summary of the critical stress and energy release rate of interfacial fracture can be found in Table 5.

RSC Advances Accepted Manuscript

This journal is © The Royal Society of Chemistry 2014

Table 5. Critical stress and energy release rate of the samples

Sample code	Material	Deposition temperature (°C)	Target thickness (nm)	Critical Stress (MPa)	Energy Release Rate (J/m^2)
TL100	TiO_2	110	100	28.7±2.0	6.5±2.0
TM100	TiO_2	200	100	31.6±3.8	1.6±0.6
TH100	TiO_2	300	100	52.8±6.0	1.8±0.5
AL100	Al_2O_3	110	100	25.6±1.6	5.3±2.4
AM100	Al_2O_3	200	100	34.7±6.4	6.0±1.3
AH100	Al_2O_3	300	100	29.2±2.6	4.5±1.4
TL300	TiO_2	110	300	62.5±7.3	11.5±5.2
TM300	TiO_2	200	300	51.7±4.7	9.1±4.3
TH300	TiO_2	300	300	50.0±6.8	7.5±1.5
AL300	Al_2O_3	110	300	36.2±6.2	3.3±2.8
AM300	Al_2O_3	200	300	48.1±3.1	7.3±4.5
AH300	Al_2O_3	300	300	60.5±5.0	8.0±5.4

Conclusions

An improved measurement system for interfacial mechanical testing of especially ALD thin films was demonstrated with quantitative capabilities. Silica microspheres were embedded in 12 different ALD coatings and the interfacial mechanical properties were studied by detaching the spheres and measuring the detaching force, area of interfacial fracture, work and energy release rate of interfacial fracture. The stress distribution was also modelled using Finite Element Analysis showing good agreement with the modelled stresses and the actual interfacial fractures. Interfacial fracture from the film-substrate interface occurred only for TiO_2 deposited at 200°C which had crystalline structure with the biggest grain size, signifying that for all of the other samples, film adhesion was excellent, and significantly better than film cohesion. Quantitatively this means that thin film interfacial adhesion to the substrate was also higher than the values of the critical stresses and the measured energy release rates. Interfacial toughness seems to be related to film thickness and crystallinity in the case of TiO_2, but with Al_2O_3 the interfacial toughness seems to increase with the deposition temperature. The method presented in this paper is generic and it can be used for the evaluation of interfacial mechanical properties, such as adhesion, between any various substrate/thin film/sphere systems of choice.

Acknowledgements

This work has been conducted within the MECHALD project funded by TEKES (the Finnish Funding Agency for Technology and Innovation). Thank you to Dr. Nora Schreithofer for the AFM-measurements. Big thanks to the workshop of the Department of Materials Science and Engineering in Aalto University: Aarno Vuorimies for manufacturing the adapter piece for the force sensor and Seppo Jääskeläinen for making it happen. Thanks to Micronova Nanofabrication Center of Aalto University for enabling all of the cleanroom fabrication. Thanks to Oskari Elomaa and Sari Sirviö for the comparative evaluation of interfacial coupling adhesion. Thanks to Ajai Iyer, Vera Protopopova and Jarmo Leppäniemi for scientific support and advice. And finally thank you to Hanna Aav for larger scale perspective and support. And hugs to my mom.

Notes and references

[a] Aalto University, Department of Materials Science and Engineering, P.O.Box 16200, 00076 Aalto (Espoo), Finland.
[b] Aalto University, Micronova Nanofabrication Center, P.O.Box 13500, 00076 Aalto (Espoo), Finland.
[c] Aalto University, Department of Electrical Engineering and Automation, P.O.Box , 00076 Aalto (Espoo), Finland.
*corresponding author e-mail: jussi.lyytinen@aalto.fi

1 S.M. George, *Chem. Rev.*, 2010, **110**, 111-131;
2 R.L. Puurunen, *J. Appl. Phys.*, 2005, **97**, 121301;
3 R.L. Puurunen, H. Kattelus, T. Suntola, in: V. Lindroos, M. Tilli, A. Lehto, *Handbook of Silicon Based MEMS Materials and Technologies, edited by T. Motooka, (William Andrew Publishing, Boston),* 2010, **1st ed** , pp. 433–446;
4 K. L. Mittal, *Electrocomp. Sci. Tech.* 1976, **3**, pp. 21-42;
5 A. A. Volinsky, N. R. Moody, and W.W. Gerberich, *Acta Mater.*, 2002, **50**, 441–466;
6 R. Lacombe, *Adhesion measurement methods, Theory and Practice, (CRC Press, New York)*, 2006, **1st ed.**;
7 J. Chen, S. J. Bull, *J. Phys. D: Appl. Phys.*, 2001, **44**, 034001;
8 O. M. E. Ylivaara, X.W. Liu, L. Kilpi, J. Lyytinen, D. Schneider, M. Laitinen, J. Julin, S. Ali, S. Sintonen, M. Berdova, E. Haimi, T. Sajavaara, H. Ronkainen, H. Lipsanen, J. Koskinen, R. L. Puurunen, *Thin Solid Films*, 2014, **552**, pp. 124-135;
9 M. Berdova, J. Lyytinen, K. Grigoras, A. Baby, L. Kilpi, H. Ronkainen, S. Franssila, and J. Koskinen, *J. Vac. Sci. Technol. A*, 2013, **31**, 031102;
10 K. Matoy, T. Detzel, M. Müller, C. Motz and G. Dehm, *Surf. Coat. Tech.*, 2009, **204**, 878–881;
11 B. A. Latella, G. Triani and P.J. Evans, *Scr. Mater.*, 2007, **56**, 493-496;
12 J. Lyytinen, M. Berdova, S. Franssila and J. Koskinen., *J. Vac. Sci. Technol. A,* 2014, **32**, 01A102, http://dx.doi.org/10.1116/1.4827197;
13 O. M. E. Ylivaara, X. Liu, L. Kilpi, D. Schneider, M. Laitinen, J. Julin, S. Ali, S. Sintonen, E. Haimi, T. Sajavaara, H. Lipsanen, H. Ronkainen, S.-P. Hannula and R. L. Puurunen, *Baltic ALD 2014 Conference Oral Presentation,* 2014;
14 M. Laitinen, J. Julin and T. Sajavaara, University of Jyväskylä, unpublished TOF-ERDA measurements
15 C. A. Schneider, W. S. Rasband, and K. W. Eliceiri, *Nat. Methods*, 2012, **9**, 671-675;
16 A. Becker, *An Introductory Guide to Finite Element Analysis. Northgate Avenue, Bury St Edmunds, Suffolk, UK: Professional Engineering Publishing Limited,* 2004, **ISBN 1-86058-410-1,** 95-96;
17 M. Zoy and D. Yang, *Tribol. Lett.*, 2006, **22**, 189-196;
18 R. L. Puurunen, T. Suni, O.M.E. Ylivaara, H. Kondo, M. Ammar, T. Ishida, H. Fujita, A. Bosseboeuf, S. Zaima, H. Kattelus, *Sens. Actuat. A: Phys.*, 2012, **188**, 268-276;

RSC Advances Accepted Manuscript

RSC Advances
RA-ART-06-2014-005807.R1
Changes to Acknowledgements (after acceptance)
8.8.2014
Jussi.Lyytinen@Aalto.fi

Here is the modified version in the final form including changes:

Acknowledgements

This work has been conducted within the MECHALD project funded by TEKES (the Finnish Funding Agency for Technology and Innovation). Thank you to Dr. Nora Schreithofer for the AFM-measurements. Big thanks to the workshop of the Department of Materials Science and Engineering in Aalto University: Aarno Vuorimies for manufacturing the adapter piece for the force sensor and Seppo Jääskeläinen for making it happen. Thanks to Micronova Nanofabrication Center of Aalto University for enabling all of the cleanroom fabrication. Thanks to the Research Group for Physical Characteristics of Surfaces and Interfaces (PCS) at Aalto University for scientific support and advice.

RSC Advances Accepted Manuscript